Impedance Characteristics and Field Separation of Body Implanted Antennas

Qiong Wang
Chair for RF Engineering,
Communication Laboratory
Dresden University of Technology,
Dresden, Germany
+49 351 463-42387
qiong.wang@tu-dresden.de

Xiao Fang
Chair for RF Engineering,
Communication Laboratory
Dresden University of Technology,
Dresden, Germany
+49 351 463-42387
xiao.fang@tu-dresden.de

Dirk Plettemeier
Chair for RF Engineering,
Communication Laboratory
Dresden University of Technology,
Dresden, Germany
+49 351 463-33203
dirk.plettemeier@tu-dresden.de

ABSTRACT

In this paper, the input impedance characteristics variance and field region separation of the implanted antenna for body area communications are investigated. The input impedance of half wave dipole wire antenna inside the human body torso and vacuum are calculatedthrough HFSS simulation and theoretical formula. Moreover, impedance measurement results of previously proposed implanted antenna is shown in this paper. Compared with the free space/vacuum operating environment, biological tissue will dramatically shrink the input impedance and resonance frequency of the implanted antenna. On the other hand, far field separation characteristics inside biological tissue are investigated for three kinds of implanted antennas which are dielectric resonance antenna (DRA), helical antenna and discone antenna. The relationship between the receiving antenna aperture and far-field boundary are simulated. In words, this paper gives insights on the impedance variance and far field separation of the implanted antennas, which will provide reference for implanted antenna development, body area communication system design as well as antenna measurement and corresponding on-body antenna design.

CCS Concepts

• CCS → Hardware → Communication hardware, interfaces and storage → Wireless devices

• CCS → Human-centered computing → Ubiquitous and mobile computing → Ubiquitous and mobile devices → Personal digital assistants

Keywords

Implanted antenna; Impedance characteristics; Far-field boundary; Phase error.

1. INTRODUCTION

Body area communications have shown more and more important roles in supporting medical and health care services. Many promising applications have already been identified from the concept of wireless body area network (WBAN). For example, a few wireless communication solutions using radio frequency (RF) technologies have been used for a number of in-body medical sensing applications like implantable cardioverter defibrillators (ICDs), cortical implants, and wireless capsule endoscopes (WCEs). The ultra-wideband (UWB) spectrum of 3.1-10.6 GHz [1] is expected to be a promising RF solution to support wider channel bandwidths for novel applications like smart electronic pills or WCEs for therapeutic procedures in addition to diagnosis. WCE capsule can take pictures/videos and then transmit the real-time biological data from the inside of the gastrointestinal tract to exterior medical instruments. The current technical challenges for UWB implanted body area communications lies in the demands of deep implantation and larger bandwidth for higher-resolution video transmission. RF frontend antennas of the TX/RX system play a critical role in the high performance of the high frequency and larger bandwidth for deep implantation communication.

Antenna development for body area communications is highly subject to the surrounding operating medium, that is, the lossy biological body. In fact, wave propagation mechanisms as well as characteristics are significantly different from that in free space. For example, the dominant wave propagation mechanisms in radio frequencies for on-body transmission link could be surface waves or diffraction for LOS or NLOS links [2]. The wave propagation speed is slowed down inside the biological tissue compared to that in free space due to the high permittivity properties of the biological tissue and the corresponding wavelength will be therefore shortened. And the so-called “shortening effect/factor” is therefore often referred for the implanted antenna development [3]. Besides, wave propagation inside the biological body will endure a fast and severe decay due to the highly lossy and dispersive property of the biological tissue. Due to the specific propagation characteristics in biological tissue environment, antenna characteristics (such as input impedance, pattern, field region separation, beam width, polarization, side lobe level, gain, beam direction, radiation efficiency, etc) will not vary in the same manner as in free space/vacuum. Specific design guidance is highly advisable for antenna development for body area communications.

In this paper, we will mainly investigate the input impedance characteristics variance and field region separation of the implanted antenna for body area communications. The two antenna characteristics will be directly indicators of the surrounding medium alteration. Input impedance of the antenna will endure a dramatic change when it is submerged inside body tissue. The resonance performance will be thence changed. [4] has studied the submerged wire antenna performance in lossy environment, such as in the earth or sea. Field region separation investigation is of high importance for implanted body area communication system design, especially the corresponding wearable antenna design as well as antenna measurements. For example, for the WCEs, the implanted capsule transmitting antenna will define its own near/far field region which will influence the reaction with the on-body receiving antenna. Dimension/aperture of the on-body receiving antenna will also be subject to the field region separation of the capsule antenna.

2. Input impedance characteristics of body implanted antenna

Impedance matching is the first step in antenna development. If the antenna is barely and deeply submerged in a lossy medium (underground, submarines and biological tissue), the current decay on such an uninsulated antenna metal/wire is very rapid. In practice, an insulating layer/jacket is highly suggested. Regarding an implanted insulated wire as a coaxial transmission line with an infinite lossy outer conductor, where the surrounding lossy medium acts as the lossy outer conductor, [4] derives a theoretical model for this lossy coaxial line model. Based on the derived propagation constants for this lossy coaxial line, the input impedance and current distribution can be determined from standard transmission line theory.

In WCEs application, assuming a half wave dipole wire antenna operates inside the human body torso at 4GHz, i.e., around the center frequency of the UWB low band (3.4-4.8 GHz). Figure 1 shows the lossy transmission line model of the insulated dipole wire antenna inside human torso tissue. It consists of three layers: inner metal wire, insulating layer and surrounding biological tissue. The surrounding tissue layer acts as the lossy outer conductor of the transmission line model, with a certain dielectric permittivity. Table 1 gives the electromagnetic parameters of the insulated dipole model inside human torso tissue at around 4 GHz. The insulating layer will be kind of polyethylene and the torso tissue will have the averaged muscle dielectric properties. In this table, r is the propagation constant, δ is the skin depth and a_3 is the attenuation constant in the human torso tissue, a_0 and a_i are the outer and inner radii of the insulating layer.

The propagation constant of the implanted transmission line can be approximated as follows [4]:

$$r \approx r_2\left(1-\frac{\frac{j\pi}{4}+\ln\sqrt{2}(0.89)^{a_0/\delta}}{\ln(a_0/a_i)}\right) \qquad (1)$$

The approximation of the propagation constant of the lossy transmission line model depends on the restriction that the intrinsic propagation constant for the biological tissue is much greater than the transmission line propagation constant, that is, $r_3 >> r$. Besides,

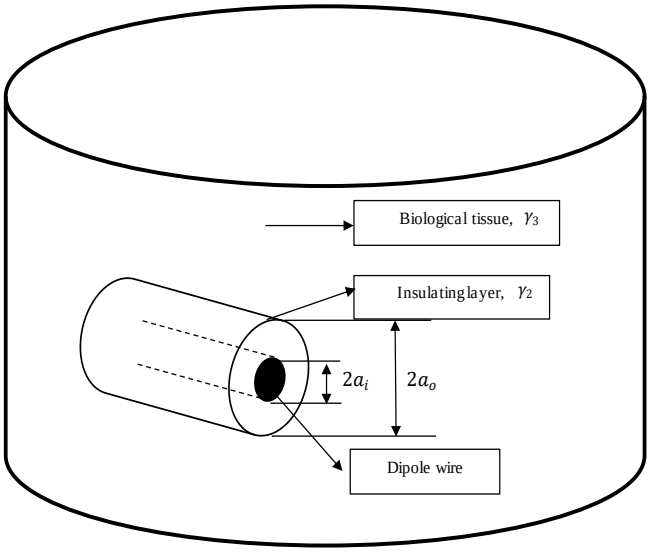

Figure 1. Lossy transmission line model of an insulated dipole inside human torso tissue

Table 1. Electromagnetic parameters of the implanted lossy transmission line model

	Insulating layer/jacket	Biological tissue (averaged body torso)
Propagation constant and related Parameters	$r_2=\sqrt{-\omega^2\mu_2\varepsilon_2}$ $\mu_2=\mu_0$ $\varepsilon_2=\varepsilon_0\varepsilon_{2r}$ $\varepsilon_{2r}=2.25$ (polyethylene)	$r_3=\sqrt{-\omega^2\mu_3\varepsilon_3}=\alpha_3+j\beta_3$ $\mu_3=\mu_0$ $\varepsilon_3=\varepsilon_0(\varepsilon_{3r}-j\frac{\sigma_3}{\omega\varepsilon_0})$ $\varepsilon_{3r}=51.4$ $\sigma_3=3.2$ $\delta=\frac{1}{a_3}$ $a_3=\omega\sqrt{\frac{\mu_3\varepsilon_0\varepsilon_{3r}}{2}\left[\sqrt{1+\left(\frac{\sigma}{\omega\varepsilon_0\varepsilon_{3r}}\right)^2}-1\right]}$

the approximation should be good if $a_0 < \delta/10$. Assume that the dipole is deeply implanted and with insulated end, the input impedance of the transmission line is

$$Z_{OC} = Z_0 \coth rl \qquad (2)$$

where l is the length of the line section which is half length of dipole antenna and Z_0 is the characteristic impedance:

$$Z_0 \cong \left(\frac{\frac{1}{2\pi}\ln a_0}{a_i}\right)\frac{r}{j\omega\varepsilon_2} \qquad (3)$$

For the biological torso tissue, the averaged dielectric properties are constant as shown in Table 1. The skin depth δ of the torso tissue at 4 GHz is derived as around 12mm. We choose an reasonable insulating jacket radius to be $a_0 = 0.1mm$ to satisfy the approximation limitation $a_0 < \delta/10$. Figure 2 shows the comparison

of HFSS simulated and calculated impedance of an implanted half wave dipole wire antenna inside the human body torso around 4 GHz and a close agreement can be seen. In fact, the approximation calculation also has been validated based on comparison with measured dipole impedance [4]. Compared to the dipole input impedance in free space, it can be concluded that the resonance impedance of the implanted dipole antenna has been reduced (from 73 Ohm to around 40 Ohm) and the resonance frequency also shifts down (from 4 GHz to 1.2 GHz).

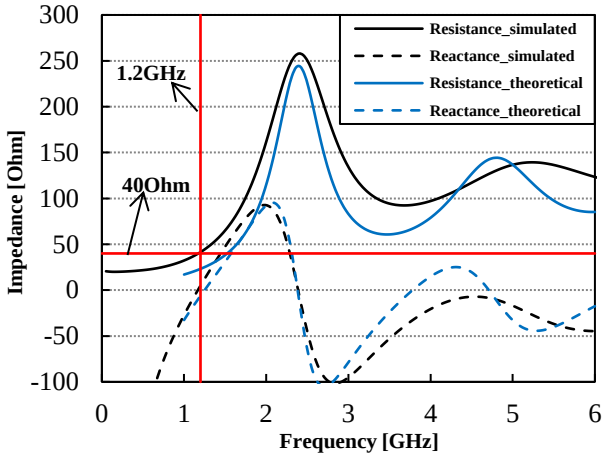

Figure 2. Comparison of simulated and theoretically calculated impedances for deeply implanted dipole with 0.1 mm polyethylene insulating jacket

In fact, input impedance of the free space antenna will endure a dramatic change when it is submerged inside body tissue. At first, we assume the body tissue is with no loss, i.e,. kind of ideal dielectric with certain high dielectric permittivity property. Figure 3 shows the simulated impedance variance of 4 GHz dipole in vacuum and when it is submerged in ideal dielectric. Both resistance and reactance parts show a sharp decline. The influence of the high permittivity property of the biological tissue lies in: reduce the overall input impedance, shift down the resonance frequency and the resonance impedance. Figure 4 further compares the impedance variance when the 4 GHz dipole is implanted in real biological torso tissue with polyethylene insulating jacket. Due to the influence of the insulating jacket, the impedance and resonance frequency shift-down becomes alleviative compared with that of directly implanted in ideal dielectric. In words, the influence of the insulating jacket lies in: increase the overall impedance, shift up the resonance frequency and the resonance impedance.

Meanwhile, in terms of the results in Figure 4, the overall input impedance has been largely decreased when the free space dipole antenna implanted inside biological tissue. In fact, in terms of dipole wire antenna, the implantation/submergence process will largely decrease the overall/resonance impedance as well as the resonance frequency. The intrinsic wave impedance of the operating medium shrinks a lot. In free space, the intrinsic impedance is $\eta = \sqrt{u_0/\varepsilon_0}$ while in biological tissue it changes to $\eta = \sqrt{\mu_0/\varepsilon_3} = \sqrt{\mu_0/\left(\varepsilon_0/\varepsilon_{3r} - j\,\sigma_3/(\omega\varepsilon_0)\right)}$ which will be much smaller than the free space wave impedance. Input impedance of the dipole wire antenna is proportional to the wave impedance of the operating environment [5]. Therefore, decline of the overall input impedance as well as the resonance impedance can be expected. In fact, beside the impedance variance due to implantation/submergence, vicinity effect is also widely investigated, for example, ground effects of lossy electric conducting surface [5], where half space effect can be interpreted although it is not fully submerged/implanted.

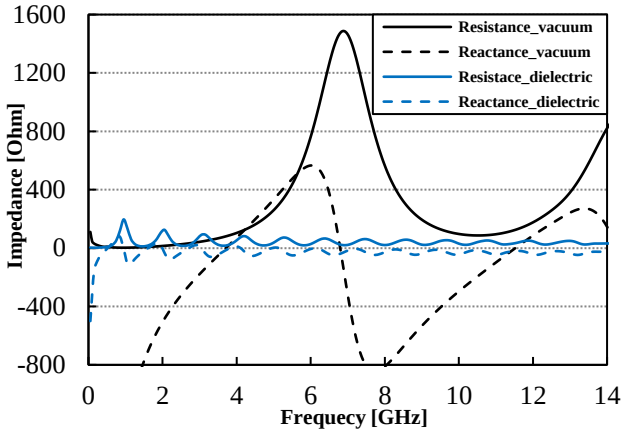

Figure 3. Comparison of the dipole impedance in vacuum and in ideal dielectric

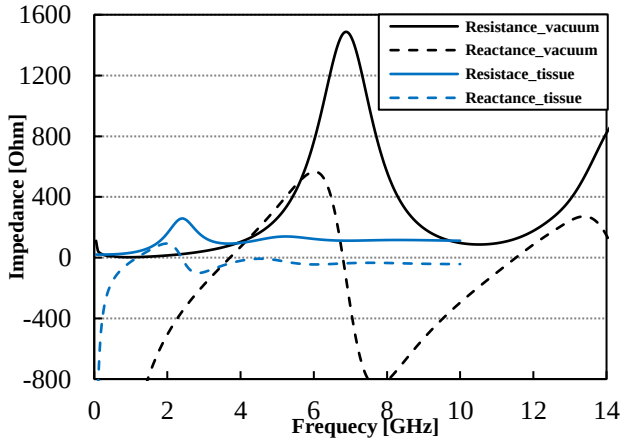

Figure 4. Comparison of the dipole impedance in vacuum and in biological tissue

Figure 5 compares the influence of three different insulating materials (air, Teflon, polyethylene) on the dipole resonant resistance and resonant frequency. The thicker the insulating thickness, the higher the resonant frequency and the resonant resistance. Teflon (with permittivity 2.1 and loss tangent 0.001) and polyethylene (with permittivity 2.25 and loss tangent 0.001) give almost the same performance. The high variance sensitivity comes from the fine wire radius a_i as well as the ratio of insulating thickness and wire radius (embodied in a_0/a_i). Besides, the resonant resistance and frequency with air insulating layer are higher than that with normal insulating dielectric layer like Teflon and polyethylene. That is due to the phase constant of air is smaller than that of Teflon and polyethylene. In fact, the phase constant of the whole implanted antenna is typically several times greater than that of the insulating layer which itself is greater than in free space.

That is why the resonant lengths of implanted antennas are typically much smaller than in free space.

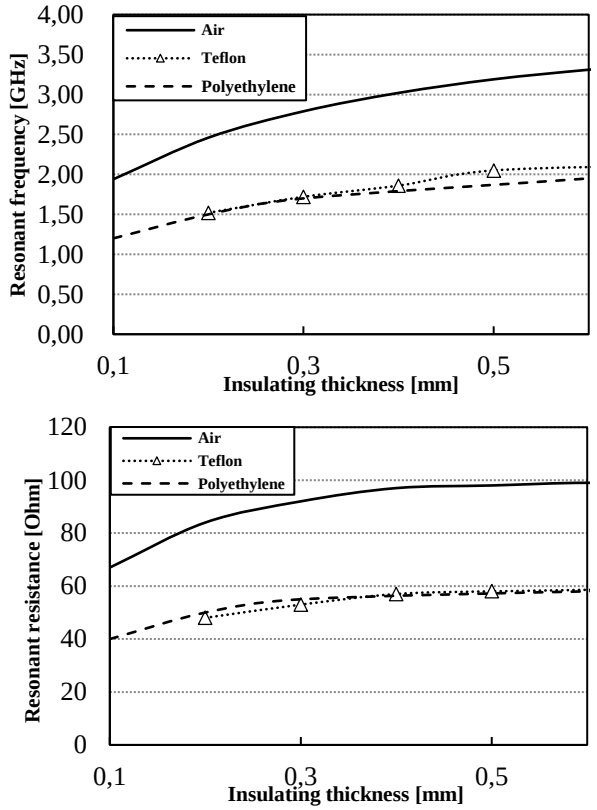

Figure 5. Implanted dipole resonance resistance and resonance frequency with different insulating materials (air, Teflon, polyethylene) and different insulating thickness.

Figure 6 shows the measured input impedance of the previously developed DRA antenna for WCE [3] in free space as well as inside body phantom. As expected, an overall/resonance impedance shrink phenomenon can be observed when it is implanted in phantom. Similar to wire antenna, the declined intrinsic wave impedance of the operating medium results in the declined antenna input impedance. In practice, antenna development for implanted antenna must take the input impedance variance as well as the shortening effect into account.

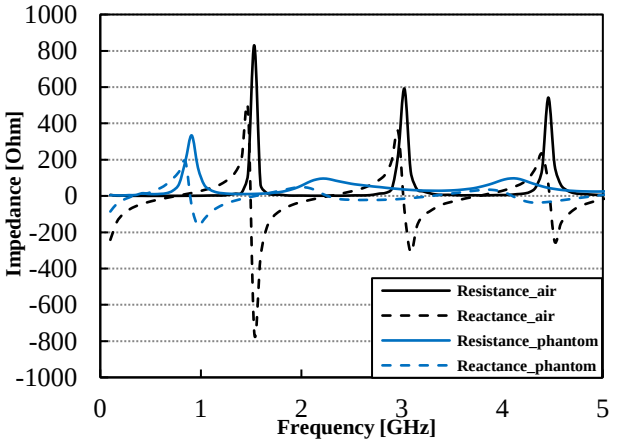

Figure 6. Measured impedance for DRA antenna in free space and inside body phantom

3. Field region separation of body implanted antenna

The space surrounding an antenna is usually subdivided into three regions: reactive near-field, radiating near-field (Fresnel) and far-field (Fraunhofer) regions [5]. The field region separation for implanted antenna is of importance especially when it comes to antenna measurements and corresponding wearable antenna development. The boundaries separating these regions are not unique, although various criteria have been established and are commonly used to identify the regions [5]. Many investigators have shown through numerous examples that a maximum total phase error of $\pi/8$ rad (22.5°) can be acceptable as a practical criterion for most practical antennas with overall length greater than a wavelength ($l > \lambda$). In spite of various criteria, a maximum total phase error of $\pi/8$ rad (22.5°) can be approximately used to identify the far-field region for implanted antennas.

In the WCE communications, the transmitting antenna is confined within possible region 10x10x5 inside the capsule (overall dimension around 11x22 mm). The implanted depths (from torso surface to the capsule) can range from 5 cm to 40 cm depending on the localization position of the capsule through the digestive tract especially the small intestine. The receiving wearable antenna can be expected on body torso surface with a relative large dimension where the antenna dimension/volume is not as demanding as the implanted capsule antenna. Strictly speaking, in terms of the WCE communications, the far-field region investigation of the implanted antenna should be combined with the aperture of the wearable receiving antenna.

In order to provide reference for the antenna measurement and the receiving antenna development, investigation on the relationship between the far-field boundary on receiving antenna aperture is of high importance for implanted body area communication system design. Figure 7 shows three different capsule antenna models operating in UWB low-band in HFSS: DRA antenna, helical antenna and discone antenna. The central operating frequency of them is around 4 GHz. The detailed descriptions of the three antennas can be found in [6]

The models of DRA antenna, discone antenna and helical antenna in HFSS are shown in Figure 7, their resonant frequencies are identical to 4GHz. These antennas are implanted in the tissue whose relative permittivity ε_r =51.4 and conductivity σ =3.3.

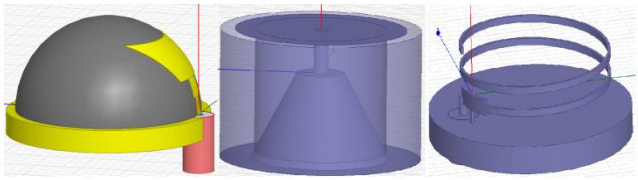

(a) DRA antenna (b) Discone antenna (c) Helical antenna

Figure 7. The HFSS models of DRA antenna, discone antenna and helical antenna

Figure 8 shows the rendering image of electrical phase of DRA antenna. The effective wavelength at 4 GHz in body torso (average

relative permittivity ε_r =51.4 and conductivity σ =3.3) is around 10 mm. As shown in Figure 8, with the increasing of implanted distance and size of receiving antenna aperture, the arc of electrical phase become smaller, which means the phase difference distributing on the aperture of receiving antenna become smaller.

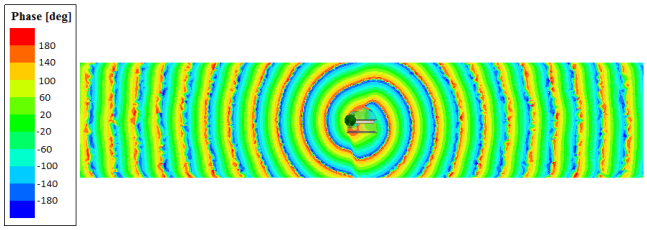

Figure 8. The phase distribution of DRA antenna simulated by HFSS

Figure 9 shows the simulated phase error of the implanted DRA antenna with variance of implanted depth r as well as receiving antenna aperture D. D/λ is the ratio of implanted depth. The effective wavelength and electrical characteristics of body torso is identical with Figure 8. The receiving antenna aperture D varies from 12mm to 40mm with spacing step 4mm. As shown in Figure 9, under the condition that receiving antenna aperture is 12mm (similar aperture as the implanted antenna), far-field boundary with phase error of π/8 rad (22.5°) is around 6.3λ. When the aperture becomes 16mm, far-field boundary becomes around 9λ. The deeper the antenna implanted, the smaller the phase error and it approaches zero when the observation point gets close to infinity. When the far-field boundary condition becomes larger than 20λ, the phase error in all the receiving antennas shown in Figure 8 can satisfy with the limitation of π/8. In the actual measurement, in order to satisfy operating at far-field region for the standard horn antenna whose aperture is 40mm, the implanted distance of DRA antenna should be set to be larger than 20λ.

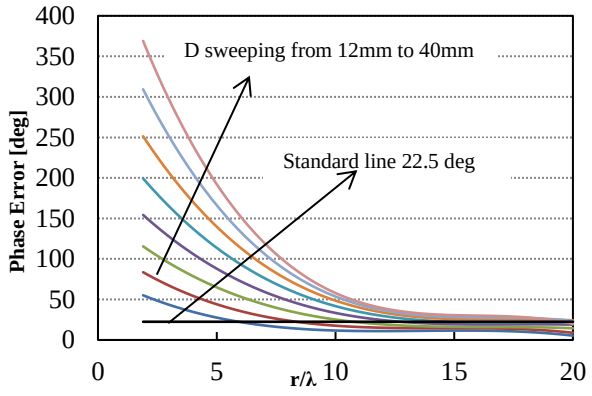

Figure 9. Relationship of phase error of DRA antenna and implanted depth with receiving antenna aperture D sweeping (effective wavelength λ around 10 mm at 4 GHz)

Figure 10 shows the phase error comparison using HFSS and CST respectively. The computational electromagnetic algorithm HFSS bases on is FEM which is a kind of frequency-domain algorithm. HFSS is beneficial to simulate some small electrical and complicated structures, and also it has great advantages in simulating antenna working at narrow bandwidth. In other way, the algorithm we used in CST is FIT which is a kind of time-domain algorithm for large space structures and antenna working at wide bandwidth. We compare the results in Figure 10, as expected, the curves got from HFSS is similar with that from CST. Due to the calculation domain of CST, we just compare the results which are limited in the domain whose size is less than 12λ.

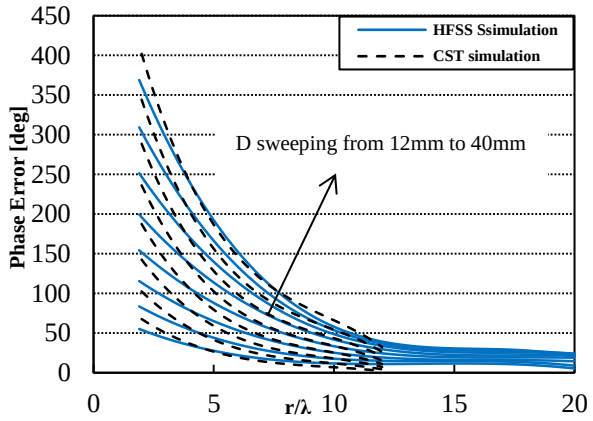

Figure 10. Simulated phase error of DRA antenna with HFSS and CST (effective wavelength λ around 10 mm at 4 GHz)

The simulation configuration of discone antenna is identical with DRA antenna: working frequency is 4GHz, efficient wavelength is 10mm, and receiving antenna aperture D varies from 12mm to 40mm with spacing step 4mm. The trend of phase error is similar with DRA antenna which also approaches to zero with increasing of implanted distance. When the implanted distance is larger than 40λ, the antennas whose aperture is less than 40mm can satisfy the limitation of phase error.

As we can see from Figure 11, phase error has raising trending after the implanted distance exceeds than 20λ. This is because that the fluctuation of phase becomes larger with the increasing of implanted distance due to the calculation error which is resulted from the limitation of calculation domain. The results shown in Figure 11 is fitted by polynomial fit technique, which means that large fluctuation result in large phase error. When the calculation domain is limited, the boundaries will influence the electrical field.

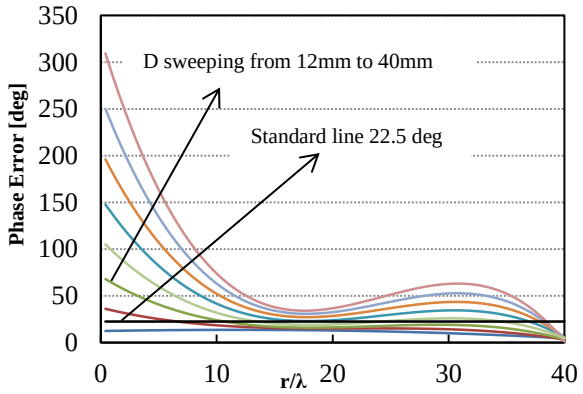

Figure 11. Relationship of phase error of discone antenna and implanted depth with receiving antenna aperture D sweeping (effective wavelength λ around 10 mm at 4 GHz)

For example, under the condition of limited height of calculation domain, the calculation error becomes larger with the increasing of

length of the calculation domain. The comparison of original curves and polynomial fitted curves is shown in Figure 12. It is obvious that the fluctuation become large after the implanted distance is larger than 20λ.

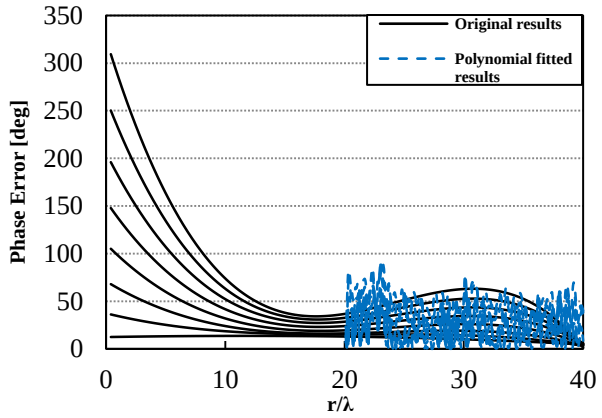

Figure 12. Comparison of original curves and polynomial fitted curves (effective wavelength λ around 10 mm at 4 GHz)

The far-field boundary of helical antenna is also simulated with configuration identical with DRA antenna and discone antenna, and the result is shown in Figure 13. Under the condition that size of receiving antenna aperture is from 12mm to 40mm, the far-field boundary starts from 2.5λ. Limited to the calculation domain, the phase distribution is confined in the region which is less than 15λ. The Figure 13 shows that if implanted distance is larger than 15λ, the receiving antenna whose aperture size is less than 24mm can satisfy the phase error requirement, which indicates that the implanted distance is at least larger than 15λ with the condition that size of receiving antenna aperture is larger than 24mm. Similar with the result shown in Figure 11, the phase error has a rising trending when implanted distance is more than 10λ. This is also because that limited calculation domain results in calculation error. Meanwhile, the negative phase error is the result of polynomial fitting.

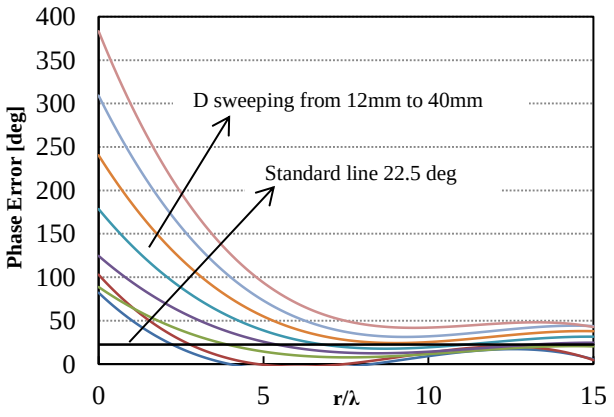

Figure 13 Relationship of phase error of helical antenna and implanted depth with receiving antenna aperture D sweeping (effective wavelength λ around 10 mm at 4 GHz)

The summarization is shown in Figure 14, which is the relationship of implanted depth with 22.5° phase error limitation and receiving antenna aperture for three kinds of antennas. As shown in Figure 14, the implanted distance increasing with the size of antenna aperture. Assuming the calculation domain with enough domain, the slop of the curves shown in Figure 14 approaches zero.

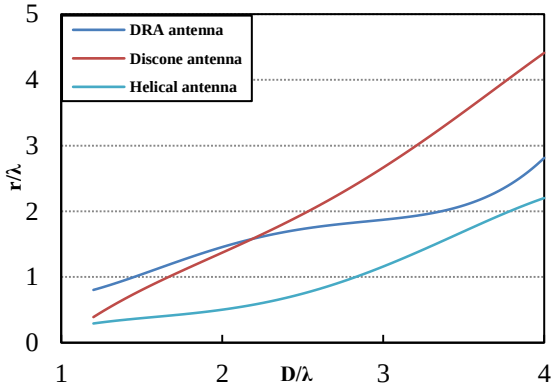

Figure 14. Relationship of implanted depth with 22.5 deg phase error limitation and receiving antenna aperture. (effective wavelength λ around 10 mm at 4 GHz)

The implanted antenna and receiving antenna are combined to calculate the wireless power transmission loss through the transmission line, which verifies the influence of implanted distance and size of antenna aperture for the transmission loss. The transmission-line mode is set operating at 3-5 GHz, center frequency at 4GHz. Discone antenna is used as the in-body transmitting antenna and Vivaldi antenna [6] is used as the on-body receiving antenna whose aperture dimension is around 40mm. Meanwhile, the implanted distance of in-body antenna is from 60mm to 85mm. The power transmission loss is simulated with different implanted distances. In order to figure out the real coupling ability of TX/RX antennas, the distance-dependent path loss is excluded from the overall transmission loss. The distance-dependent path loss can be calculated based on the path loss lognormal model [7]. Eqn.4 can calculate the path loss in human body [7]:

$$PL(d)_{dB} = PL(d_0) + 10nlog_{10}\left(\frac{d}{d_0}\right) + \sigma_s \qquad (4)$$

Where d_0 is the reference distance, n is the pass-loss exponent, and σ_s is the shadow fading, $PL(d_0) = 48.6$, n = 10.6, and $\sigma_s = 8.2$. Figure 15 shows the wireless power transmission loss excluding the distance-depended path loss. As the implanted distance increases in the range from 60mm to 85mm, coupling strong between in-body and on-body antenna become stronger.

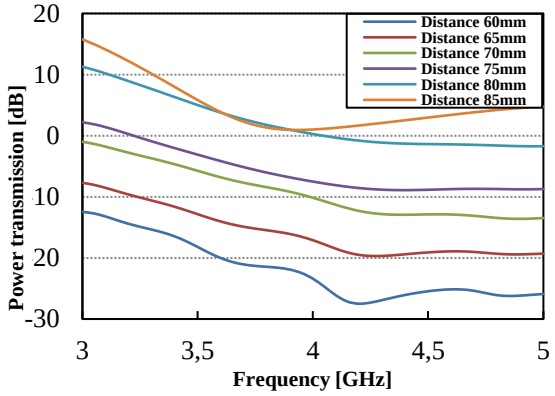

Figure 15. Wireless power transmission loss excluding distance depended path loss

From Figure 11, it is obvious that, under the condition that aperture size of receiving antenna is 40mm, phase error decreases with the growth of implanted distance. For receiving antenna operating at near field of implanted antenna, phase error distributed on the antenna aperture severely influences its ability to couple power from transmission antenna. In the process of designing on-body receiving antenna, it is of importance to sufficiently consider the implanted distance and the size of receiving antenna aperture to maximize the coupled power.

4. Conclusion

This paper analyzed the input impedance characteristics variance and field region separation of the implanted antenna for body area communications. The input impedance of half wave dipole wire antenna inside the human body torso and vacuum are calculated, separately with HFSS simulation and theoretical formula. It is obvious that input impedance of the antenna will endure a dramatic change when it is submerged inside body tissue and the resonance performance will be thence changed. And the influence of three types of insulating materials (air, Teflon, polyethylene) on the dipole resonant resistance and resonant frequency is also compared. The thicker the insulating thickness, the higher the resonant frequency and the resonant resistance. Meanwhile, the measured impedance of the previously developed DRA antenna in free space as well as inside phantom is shown. The reducing of impedance and shrinking of resonant frequency are observed from the results.

Three kinds of implanted antennas which are separately DRA antenna, helical antenna and discone antenna are investigated for their far-field boundaries satisfied $\pi/8$ rad phase error. For the constant size of antenna aperture, the trend of phase error approaches to zero with increasing of implanted distance. Phase error is also influenced by the size of aperture, which approaches zero more easier in smaller antenna aperture. Thus strictly speaking, the field separation investigation of the implanted antenna should be combined with the aperture of the receiving antenna.

The coupling ability is a significant factor evaluating the performance of receiving antenna, which is obviously influenced by phase error distributed in the antenna aperture. The field separation region calculation can be helpful reference to receiving wearable antenna development. Thus, in the process of designing on-body receiving antenna, it is of importance to sufficiently consider the implanted distance and the size of receiving antenna aperture to maximum the coupled power.

5. ACKNOWLEDGMENTS

This research is supported by "WiBEC" (Wireless In-Body Environment) project which has received funding from the European Union's Horizon 2020 research and innovation programme under grant agreement No. 675353.

6. REFERENCES

[1] FCC 2002. 02-48, Revision of Part 15 of the Commission's rules regarding ultra-wideband transmission systems.

[2] Zasowski T. , Meyer G. , Althaus F. 2006. UWB Signal Propagation at the Human Head, *IEEE Transaction On Microwave Theory And Techniques*, 54, 4 (April 2006), 1836-1845. DOI=http://doi.acm.org/10.1109/TMTT.2006.871989.

[3] Wang Q., Wolf K., and Plettemeier D. 2010. An UWB capsule endoscope antenna design for biomedical communications. In *3rd International Symposium on Applied Sciences in Biomedical and Communication Technologies* (Rome, Italy, November 07-10, 2010). ISABEL. DOI= http://doi.acm.org/10.1109/ISABEL.2010.5702832.

[4] Fenwick R. and Weeks W. 1963. Sumberged antenna characteristics. *IEEE Transactions on Antennas and Propagation*, 11, 3 (May 1963), 296-305, DOI=http://doi.acm.org/10.1109/TAP.1963.1138035.

[5] Balanis C. A. 2005. *Antenna Theory: Analysis and Design, 3nd Edition*, Wiley, New Jersey.

[6] Anzai D., Katsu K., Chavez-Santiago R., Wang Q., Plettemeier D., Wang J., Balasingham I. 2014. Experimental evaluation of implant UWB-IR transmission with living animal for body area networks. *IEEE Trans. Microwave Theory Tech.*, 62, 1 (Nov 2013),183–192, DOI=http://doi.acm.org/10.1109/TMTT.2013.2291542.

[7] Wang J., Wang Q. 2012. *Body Area Communication: Communication Systems, and EMC*, Wiley, USA, NJ.